Calibration of the Neutral Particle Imager for the Aspera-3 Instrument

K. Johnsson[1], K. Asamura[2], S. Barabash[1]

December 12, 2003

1. Swedish Institute of Space Physics (IRF), Sweden.
2. Institute of Space and Astronautical Sciences (ISAS), Japan.

Abstract

This report treats the functional test and calibration of the Neutral Particle Imager (NPI), which is a part of the instrument ASPERA-3 to be flown on Mars Express. For the functional test the detector MCP (Micro Channel Plate) saturation voltage and dark current are measured. A drift in NPI channel with MCP bias voltage was discovered in the NPI. Preliminary analysis suggests that a large area charge cloud ($\approx$13 mm in diameter) covering several channels is formed at the MCP surface when high MCP bias is used. Further investigation of this effect is needed. For the calibration part of the sensor efficiency and response to azimuth and elevation scans are presented. Finally, the geometrical factor of the sensor is evaluated to $2.7 \cdot 10^{-3}$ cm^2 sr.

1 Introduction

The ASPERA-3 instrument will investigate plasma-neutral interactions near Mars as part of the Mars Express mission scheduled for launch 2003. ASPERA-3 includes the Neutral Particle Imager (NPI) which is will image energetic neutral atoms (ENA) with an angular resolution of 11.25°. The NPI is a cylindrical tophat type instrument with 32 apertures. A high voltage deflection system will remove charged particles from the measured flux so that only neutral particles can pass the deflection system and impact a tilted target block. Secondary and reflected particles are converted to a current pulse with a Multi Channel Plate (MCP) chevron configuration. At the MCP output a sectioned anode connected to front end electronics

1.1 Description of the Calibration Facility at IRF

The system in the IRF laboratory is the Model 2751 50 keV Ion Source from Peabody Scientific. It is capable of producing a parallel and even ion beam with an energy of up to 50 keV/q. The system can be run in three different modes to be able to achieve the three energy ranges 0 - 1 keV/q, 1 - 15 keV/q and 15 - 50 keV/q. Ions are produced in the duoplasmatron from arcing between an anode and an oxide coated mesh filament. There is a funnel-shaped electrode constricting the gas and generated plasma cloud to a volume that is converging toward the axial aperture exit. This restricts the plasma to a narrow beam emerging from the aperture. To increase the ionization efficiency, a strong magnetic field is applied in the axial direction of the duoplasmatron. Electrons generated will then spiral along the magnetic field lines towards the anode and produce longer ionization tracks. The ion beam is then extracted through an

extraction gap by an extraction electrode and then accelerated through a three-element Einzel focusing lens, which also helps to collimate the diverging ion beam into a parallel beam. The focal length can be optimized by adjusting the lens voltage. The ions then enters an ExB filter. This consists of a perpendicular magnetic and an electrical field. The electrical field strength can be varied to filter out the desired ion mass according to the formula: The electrode voltage is divided between the voltage on the top electrode (V^{+}_{ExB}) and the voltage on the bottom electrode (V^{-}_{ExB}). These are not perfectly symmetrical. After exiting the ExB filter the ions are accelerated in an acceleration gap to achieve the final beam energy. The beam is then further filtered through the electrostatic analyzer, which is a 90 degree spherical electrode with a radius of 5 ". Ions with energies different from the energy selected by setting the electric field inside the analyzer will not make the turn. The ESA at the IRF facility has an energy resolution of 1 %. To permit widening of the ion beam emerging from the ESA, the defocus lens first diverges the beam and then the focus lens collimates the diverging beam into a parallel beam leaving the system. Both lenses are three-element Einzel lenses of different size. The retractable Faraday cup provides measurements of the beam intensity and because of this also indirectly the beam location. It is mounted inside the vacuum tank.

2 Functional Test of the NPI Flight Model

The functional test of the NPI sensor was designed to verify the basic functionality of the sensor, measure the MCP-bias saturation voltage and measure the sensor dark response.

2.1 MCP Bias-Channel Effect

Initial function tests revealed what looked like a channel drift effect when high MCP bias is applied. Figure 1 shows the instrument response for an H_2^+ beam incident on channel 2 (neighboring channels were covered with Al-foil as depicted in the instrument setup in figure 9b). The graphs show the normalized count rate versus channel number for different MCP bias. There is a clear drift present in channel with higher MCP bias.

The NPI electronics has a programmed priority for dealing with counts that occur within a short time period (200 ns) on two different channels. In the event that this happens, the count is given to the higher channel. With this in mind the drift could be explained as large area (spanning across channel boundaries) charge cloud forming in the MCP region. This in turn would cause simultaneous impacts on the anode and because of the channel priority this would then be manifested as a channel drift to a higher channel. There is another possibility however that the effect is caused by crosstalk between neighboring channel anodes. The signal on one sector anode could be coupled to neighboring anodes and this drift effect would again result from the channel priority.

To verify whether this cloud exists or not, the deflector and lid of the NPI was removed and the sensor was mounted perpendicular to the ion beam (as in figure 12c). The count rates were then measured at three different positions, A, B and C (figure 2), along the central line of channel 16, where A was near the center (where the anode sectors are small and therefore also closer together), B was half way between edge and center, and C was near the edge of the MCP (where the anode sectors are wide). The MCP bias for all measurements was 2700 V. If there existed a cloud with an area large enough to cause the channel drift, the measurement at point C would have a smaller drift associated with it than the measurement at point A where a cloud would cover more channels. The result in figure 3a, where the channel average based on normalized count rate is plotted for the three points, suggests that this is the case. Close to the center of

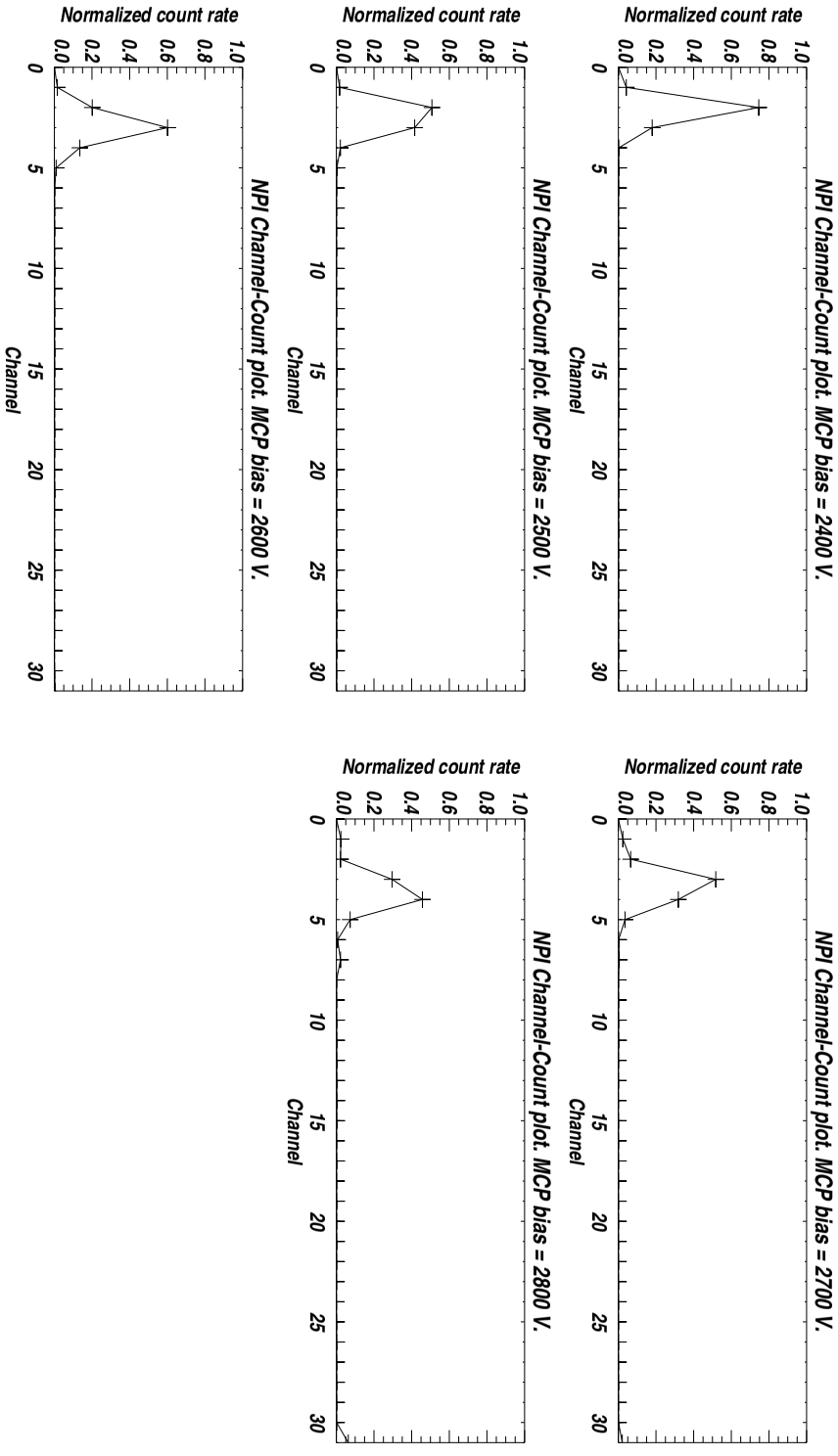

Figure 1: Normalized count versus channel. The target channel drifts to a higher channel with increased MCP bias.

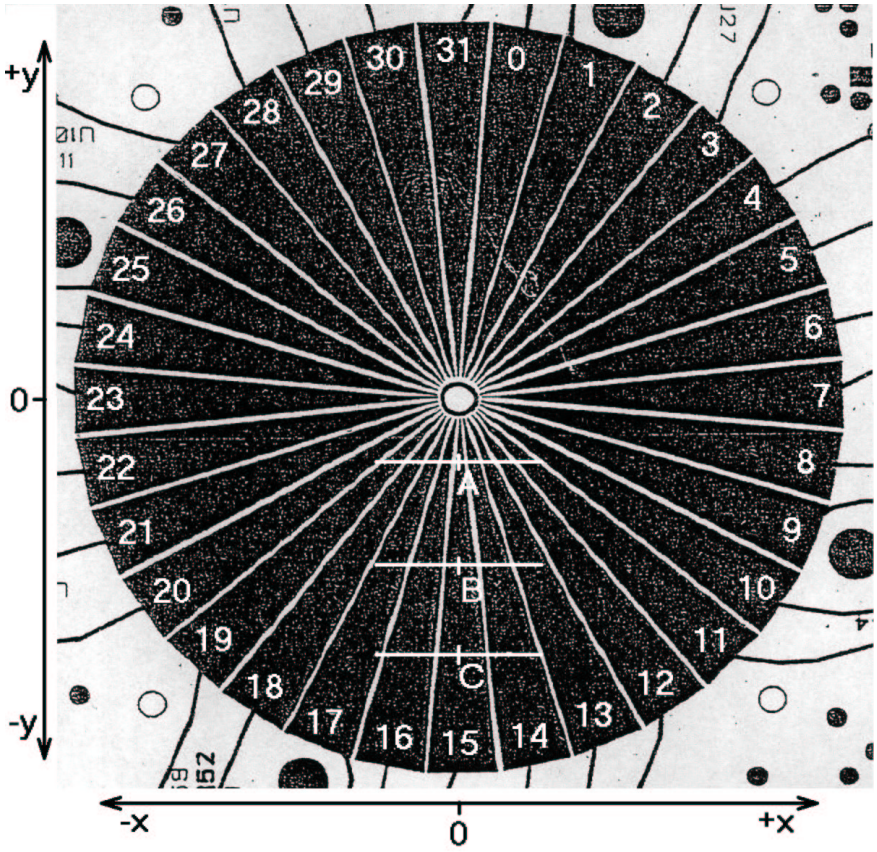

Figure 2: NPI anode sectors. channel numbers have been added. The white horizontal lines at positions A, B and C are all 13 mm.

the MCP the count rate median was between channels 16 and 17 while close to the edge it is between channels 17 and 18. Since, in a crosstalk situation the drift effect should be independent of where on the anode the electrons hit, this result supports the charge cloud theory.

If this indeed is a real charge cloud with large area formed in the NPI at high MCP bias a very rough estimation of its size can be made from scans over channel boundaries at low MCP bias and then adding a measured size difference. The estimation is based on a method by Edgar et al (1989) to investigate the radial charge cloud distribution between MCP output and a split strip anode.

Because of the symmetry of the anodes of two neighboring channels, measuring the fraction of count rates for one channel to its neighbor at different points across a channel boundary will produce the S-shaped curves in figure 3b. The channels used are 6, 7 and 8 for a vertical scan and 15, 16 and 17 for a horizontal scan. The charge distributions in the x and y direction (x and y is defined as in figure 3) is found from the derivative of the S-curves. This method is used to roughly estimate the size of the charge cloud at low MCP bias only. Because of the priority in the NPI electronics the fraction of counts on any side of the channel boundary will not be correct. However, the error will be less for a small area cloud than for a large area cloud (because fewer charges in the cloud would produce fewer coincidence counts). After estimation of the cloud size at low MCP bias the vertical and horizontal scan measurements gives the difference between the two charge cloud radii (the difference in position when counts are first detected in the higher channel for high and low MCP bias).

Figure 3c is a plot of the charge distribution for the low MCP bias charge cloud from scans in x and y directions (x is the dotted line). From this plot it is suggested that though the charge cloud is not perfectly symmetric in the vertical and horizontal directions (lines should coincide [Edgar et al, 1989]) the estimated diameter is ≈2 mm in both directions. If the difference in cloud diameter $2 \cdot \delta y = 11$ mm from figure 3d is added the estimated charge cloud diameter for high MCP bias is ≈13 mm.

One must point out that the error present in our measurements is high because of the priority of the NPI electronics (which causes the S-curves to rise faster) and the fact that the channel boundary is inclined (22.5° for the vertical scan and 5.6° for the horizontal) to the scan vector (which causes the S-curves to rise slower).

The approximation of 13 mm cloud diameter is not very consistent with the test in figure 3a. More specifically the slope of figure 3a does not seem steep enough. The figure shows where the *weight* of the counts appear for the different positions A, B and C. In fact, the highest channel which counts appear for position A is channel 20 and for B and C it is channel 19. The white horizontal lines in figure 2 are 13 mm and centered over the positions A, B and C. It is clear that a cloud size of diameter 13 mm would not reach channel 19 as the data indicates at positions B and C, while at A the data seems to correspond. For a charge cloud centered at position C to include channel 19, its diameter would have to be on the order of 30 mm. However, if the charge cloud has a 13 mm diameter and is equally distributed in x and y directions on position A it would cover the central part of the MCP and all anode sectors would have counts. With the priority a large number of these should be registered in channel 31, but as shown in figure 1, there is no response above noise level in this channel. Either the charge distribution of the cloud changes dramatically with MCP hit position or the charge cloud does not exist and something else causes the effect.

2.2 MCP Saturation

The instrument setup for the saturation measurement is in figure 11a. The measurement beam parameters were:

Species:	H_2^+
Energy:	4.8 keV
Intensity:	$0.072 \cdot 10^{-11}$ A
Channel:	8
Sampling time:	1 s
The values are	averaged over 60 s.

A plot of the measured total count rate with increasing MCP bias voltage is in figure 4. From the figure the optimal operating MCP bias voltage should be in the shoulder region of 2500 - 2600 V. However, due to the MCP bias-channel effect (section 2.1) the optimal operating MCP bias voltage cannot be used with restored angular resolution. For this reason the lower operating MCP bias voltage of 2400 V is recommended.

2.3 MCP Dark Current

A plot of the NPI dark count at different MCP bias and corresponding histogram is in figure 5. The instrument setup for the dark count measurement is in figure 11b. No beam was used in this measurement. The sampling time was 10 s and the measurement was averaged over 60 samples. The measured dark current count rates for all channels at different MCP bias are in table 1.

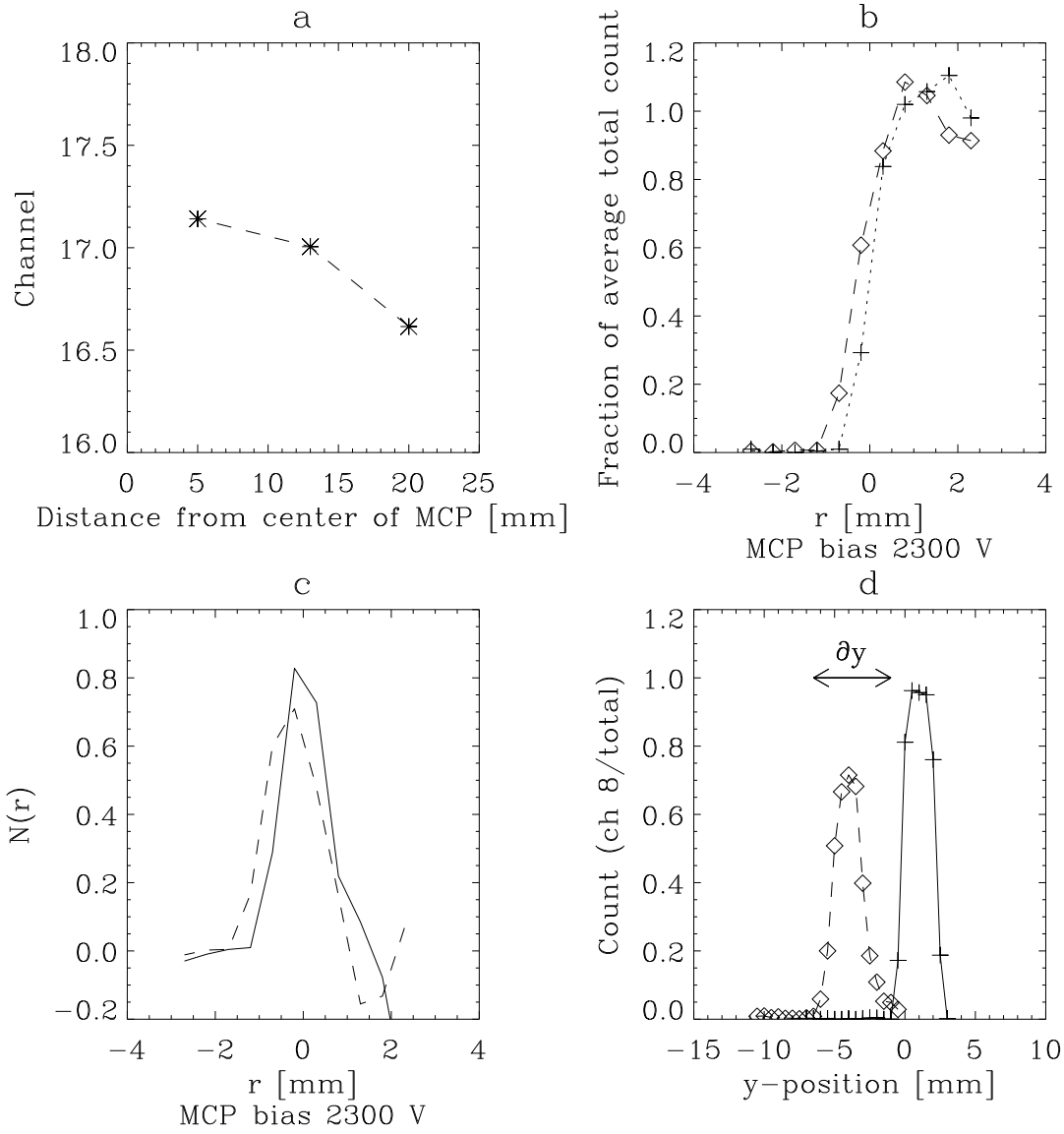

Figure 3: (a) shows the channel average from normalized count rates for three points on the MCP. The plot suggests that the channel drift is increased when close to the center of the MCP plate, a result which could be explained by more channel anodes covered by a large area charge cloud from the MCP output. The S-curves in (b) show the fraction of total count rate present in channels 7 and 8 (+) and 16 and 17 ($\diamond$) as the ion beam is moved vertically (+y direction) over channels 6,7 and 8 and horizontal (-x direction) over channels 15,16 and 17. (c) is the derivatives of the S-curves and thus the charge distribution in the vertical (full line) and horizontal (dotted line) directions. Plot (d) shows the instrument response at MCP bias 2300 V (+) and 2700 V ($\diamond$). The difference δy between the front edges of the scan (scan direction was +y) is the difference in radius between the two clouds.

Table 1: Dark count per second at different MCP bias

Channel	MCP bias 2400 V	MCP bias 2600 V	MCP bias 2800 V
0	4.0	3.9	2.9
1	6.1	6.6	4.3
2	6.9	9.7	7.6
3	6.8	10.0	9.8
4	5.5	11.6	12.0
5	5.7	11.8	12.8
6	7.1	11.6	14.9
7	4.3	11.1	15.0
8	5.5	9.4	13.9
9	5.6	10.9	14.5
10	6.9	12.7	13.9
11	5.5	11.7	13.7
12	4.9	10.5	15.7
13	6.1	10.4	13.2
14	6.0	11.5	17.2
15	4.4	11.1	14.5
16	4.7	11.9	14.0
17	5.1	10.7	13.7
18	5.1	11.0	14.6
19	4.9	11.2	15.8
20	4.6	9.3	14.5
21	4.2	11.6	14.7
22	5.3	11.5	14.8
23	4.9	9.5	11.5
24	4.6	10.2	11.7
25	6.3	11.5	12.4
26	7.3	13.0	14.0
27	6.6	13.7	12.5
28	7.6	11.5	13.3
29	7.4	12.1	13.8
30	6.4	13.3	15.2
31	7.8	25.6	47.5

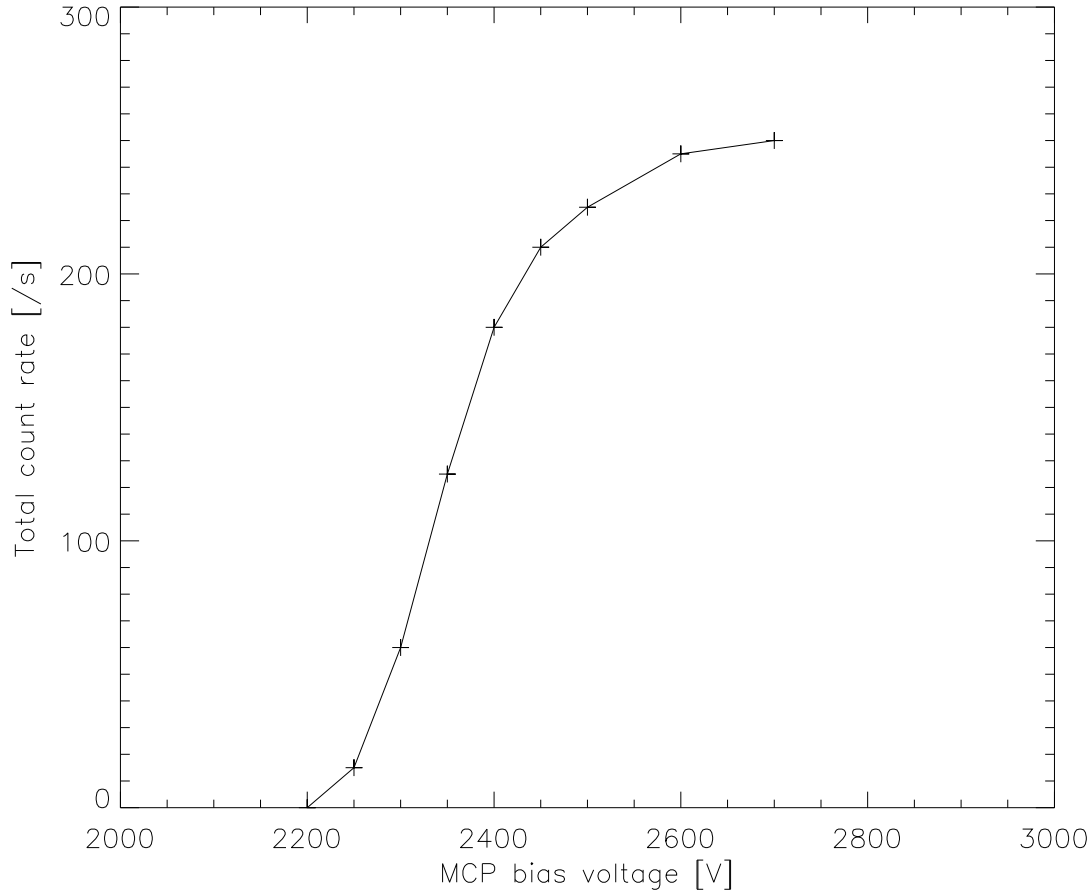

Figure 4: Measured total count rate with MCP bias voltage. This measurement was made with a 4.8 keV, H^+ beam.

3 Calibration of the Flight Model

3.1 Calibration Plan

The calibration plan of the NPI sensor includes a full investigation of the response of one sector only and then an investigation of the relative response of the other sectors. Thorough investigation of all 30 open sectors would be too time consuming. An investigation of one reference sector should include the angular response (scans of azimuth and elevation angles) at different beam energies. Also, the efficiency should be calculated for different energies Suggested beam energies are 0.5, 0.75, 1.0, 5.0 and 10 keV.

When the response from the reference sector is known, a relative response of the other sectors is found from a 360° azimuth scan with elevation angle fixed at the maximum response position.

3.2 Efficiency Measurement

The efficiency ε of the NPI sensor is measured as a count rate C over beam current I for the ratios of the beam profile area A_{beam} and the effective sector target block area of the NPI, A_{eff}:

$$\varepsilon = \frac{C \cdot A_{beam}}{I \cdot A_{eff}}, \tag{1}$$

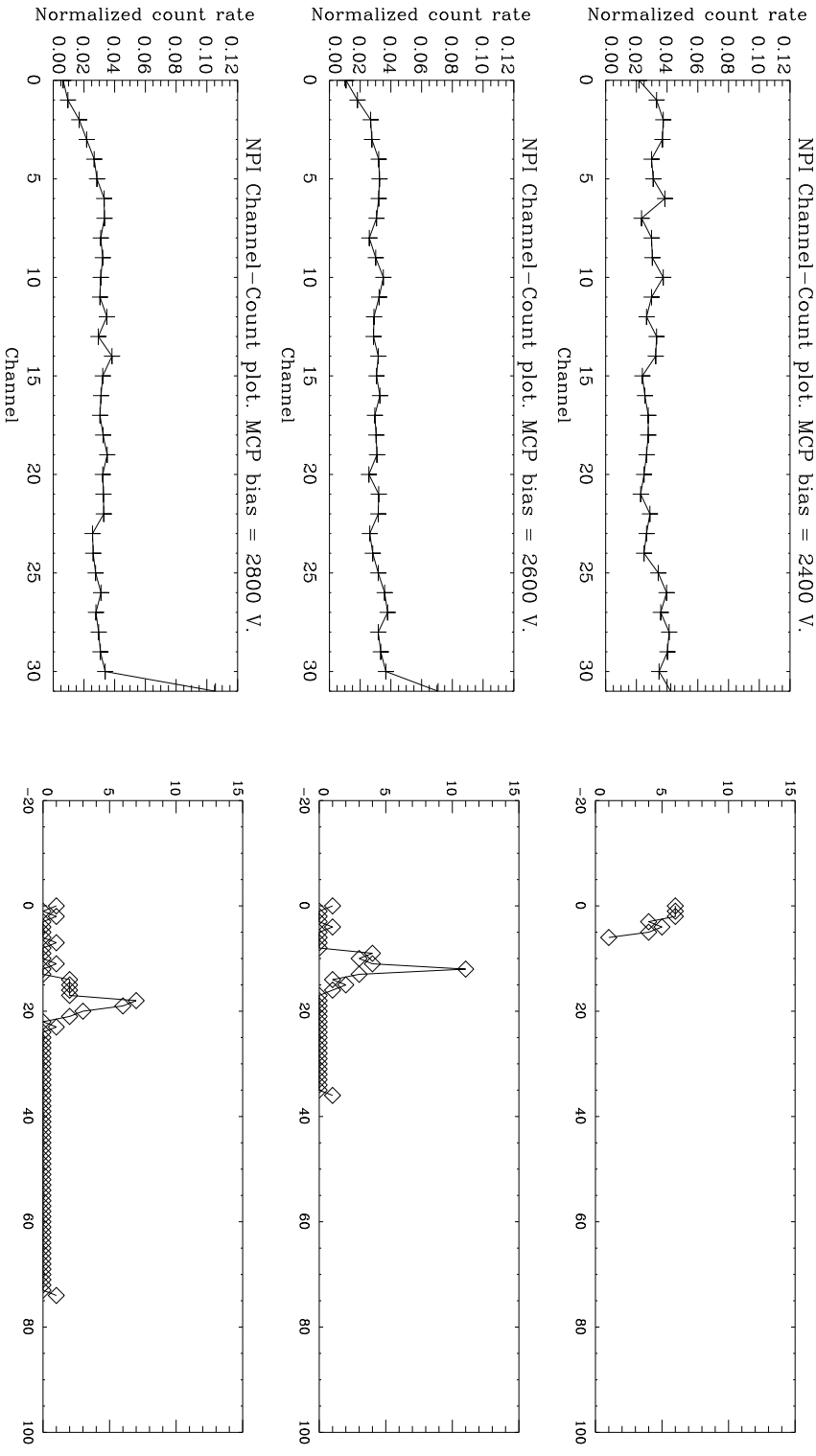

Figure 5: Normalized dark count versus channel and corresponding histogram.

Table 2: Linear coefficients for efficiency

V_{MCP} [V]	k	m
2300	$1.205 \cdot 10^{-4}$	$-1.346 \cdot 10^{-5}$
2400	$5.261 \cdot 10^{-4}$	$-1.008 \cdot 10^{-4}$
2500	$7.423 \cdot 10^{-4}$	$-1.509 \cdot 10^{-4}$
2600	$7.567 \cdot 10^{-4}$	$-1.625 \cdot 10^{-4}$

Here, the target block area, A_{eff}, is 0.128 cm^2 and A_{beam} is limited to 10.1 mm using a slit. The beam current is:

$$I = \frac{I_{faraday}}{e},$$

where $I_{faraday}$ is the Faraday cup reading and e is the elementary charge.

Efficiency measurements were made for different MCP bias and using H_2O^+ ions of different energies. The instrument configuration for these measurements is found in figure 11d and the measurement beam parameters were:

Species:	H_2O^+
Energy:	0.29, 0.48, 0.96 and 4.8 keV
Intensity:	$\approx 3 \cdot 10^{-14}$ A - $\approx 3 \cdot 10^{-13}$ A
Channel:	8
Sampling time:	30 s
The count is	averaged over 8 samples.

Figure 6 is a plot of the efficiency with linear approximations fitted. The linear coefficients for the fits are in table 2. The linear equations are of the form:

$$\varepsilon = kE + m, \tag{2}$$

where E is the ion beam energy in keV.

The choice of MCP bias for the NPI sensor is partly based on the efficiency measurement results. There is an efficiency gain of ≈ 2.4 between the results with an MCP bias of 2300 V and 2400 V for energy 0.29 keV and ≈ 4.3 for energy 9.6 keV (the difference in slope of fitted lines is 4.36). There is thus a large efficiency improvement if the NPI MCP bias is 2400 V compared to 2300 V.

3.3 Azimuth Scans

The azimuth scan response for the NPI sensor at MCP bias 2300 V is in figure 7. The deflector voltage is 1000 V, which effectively filters the majority of ions and lets the neutral constituent of the beam impact the target block. The instrument configuration for this measurement is in figure 11d and the beam parameters for this measurement was:

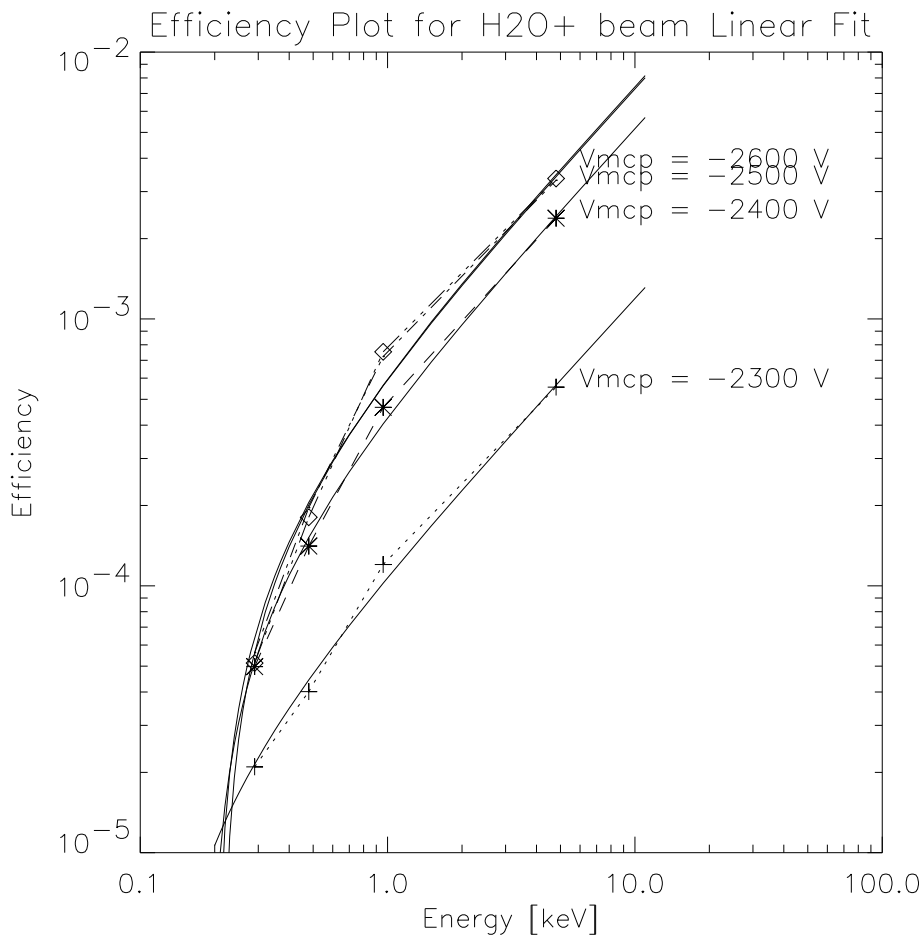

Figure 6: Efficiency using H_2O^+ ions with linear fits.

Species:	H_2^+
Energy:	9.6 keV
Intensity:	$\approx 50.0 \cdot 10^{-11}$ A
Channel:	0-31 (full scan : $\Delta\varphi = 1°$)
Sampling time:	1 s
The count is	averaged over 8 samples.

The relative response of the different sectors are in table 3. It shows the averaged response of the sector centers (azimuth center $\pm 2°$) for each channel relative to channel 8.

3.4 Angular Response

Full azimuth and elevation scans were performed on channel 14 and responses for MCP bias 2300 V was recorded. The normalized responses are in figures 8, 9 and 10 for MCP bias 2300, 2400 and 2500 V respectively. Instrument configuration is shown in figure 11d. The ion beam configurations for these measurements were:

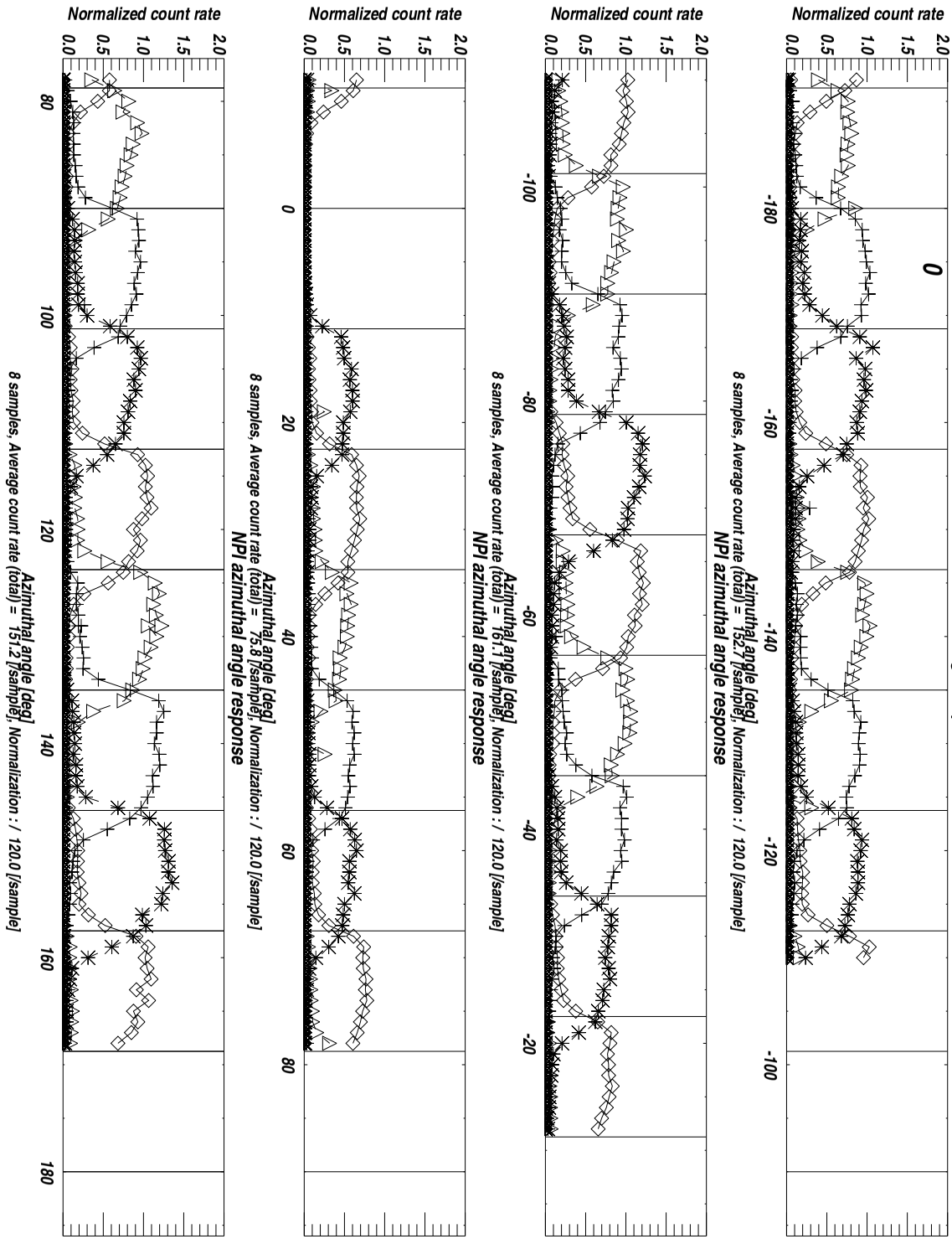

Figure 7: 360° azimuth scan of normalized sector response. The sector numbers are displayed. Measurement was made with MCP bias of 2300 V and a deflector voltage of 1000 V.

Table 3: Response (counts/s) of all channels relative to the response of channel 8

Channel	0	1	2	3	4	5	6	7	8	9	10
Relative sensitivity	1.11	1.07	1.08	1.07	1.00	0.99	1.10	1.04	1.00	1.31	1.30
Channel	11	12	13	14	15	16	17	18	19	20	21
Relative sensitivity	1.16	1.05	0.85	0.88	0.00	0.00	0.65	0.69	0.58	0.64	0.64
Channel	22	23	24	25	26	27	28	29	30	31	
Relative sensitivity	0.84	0.97	0.99	0.98	1.15	1.28	1.30	1.44	1.09	0.86	

For MCP bias 2.3 kV:

Species:	H_2^+
Energy:	9.6 keV
Intensity:	$\approx 50.0 \cdot 10^{-11}$ A
Channel:	14 (full scan : $\Delta\varphi = 1°$ and $\Delta\theta = 1°$)
Sampling time:	1 s
The count is	averaged over 7 samples.

For MCP bias 2.4 kV and 2.5 kV:

Species:	H_2O^+
Energy:	9.6 keV
the respective intensities were	$\approx 3.5 \cdot 10^{-11}$ A and $\approx 4.0 \cdot 10^{-11}$ A.
Channel:	14 (full scan : $\Delta\varphi = 1°$ and $\Delta\theta = 1°$)
Sampling time:	1 s
The count is averaged over	7 samples.

The analytical fit functions added in figures 8, 9 and 10 are not ideal and should be viewed upon with scepticism. They are based on a polynomial fit and the resulting fitted peaks are too wide. The polynomial fits are based on the function:

$$f(\varphi, \theta) = \sum k_{i,j} \cdot \varphi^i \cdot \theta^j, \tag{3}$$

where φ and θ are azimuth and elevation angles and $k_{i,j}$ is a coefficient. The values of $k_{i,j}$ for the fit in figure 8 is in table 4.

3.5 Estimation of Geometrical Factor From Measurements

The response of each sector on the NPI is defined as a count rate C = counts/s. If the effective area of one NPI sector is A_{eff} the The measured geometrical factor G is defined as:

$$G = \frac{A_{eff}(\theta_0, \varphi_0)}{C_{meas}(\theta_0, \varphi_0)} \int_\varphi \int_\theta C_{meas}(\theta, \varphi) \cos\theta d\theta d\varphi, \tag{4}$$

where A_{eff} is the effective areal size, C is the measured count rate, θ is the elevation angle and φ is the azimuth angle. The calibration data from channel 14 was used for the geometrical factor

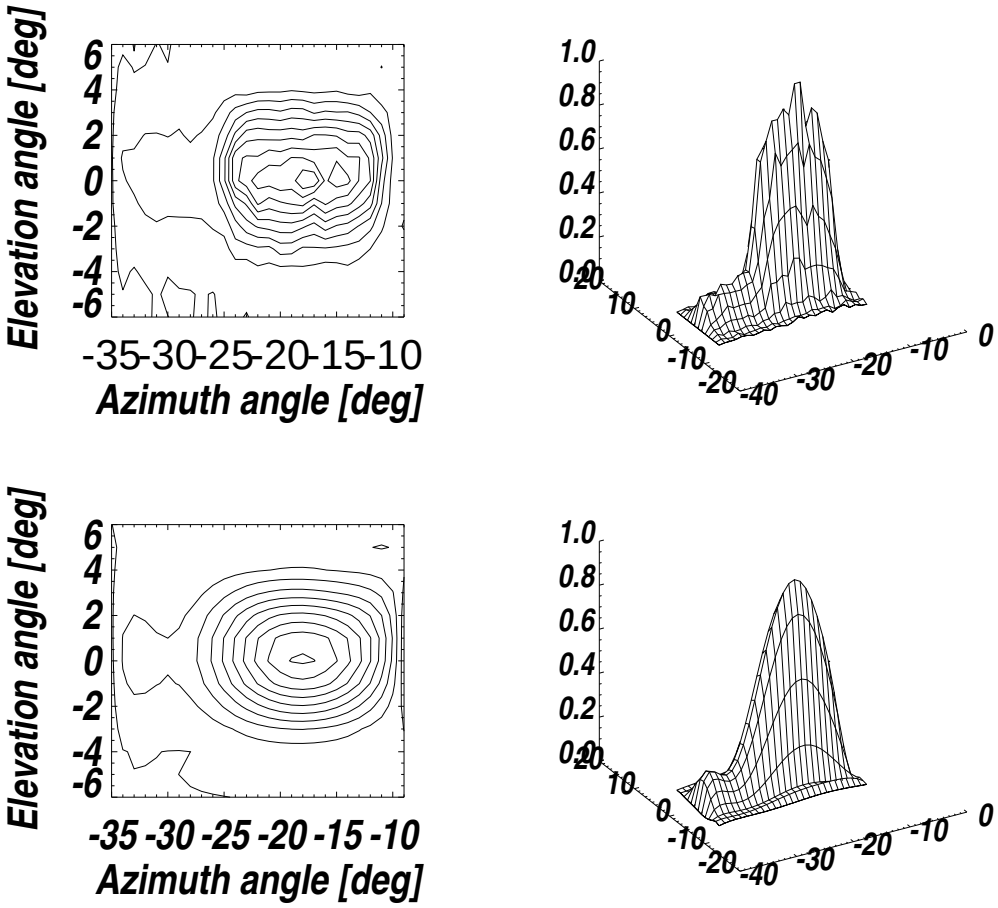

Figure 8: Angular scan of channel 14 at MCP bias 2300 V (top left and right) with corresponding fits (bottom left and right).

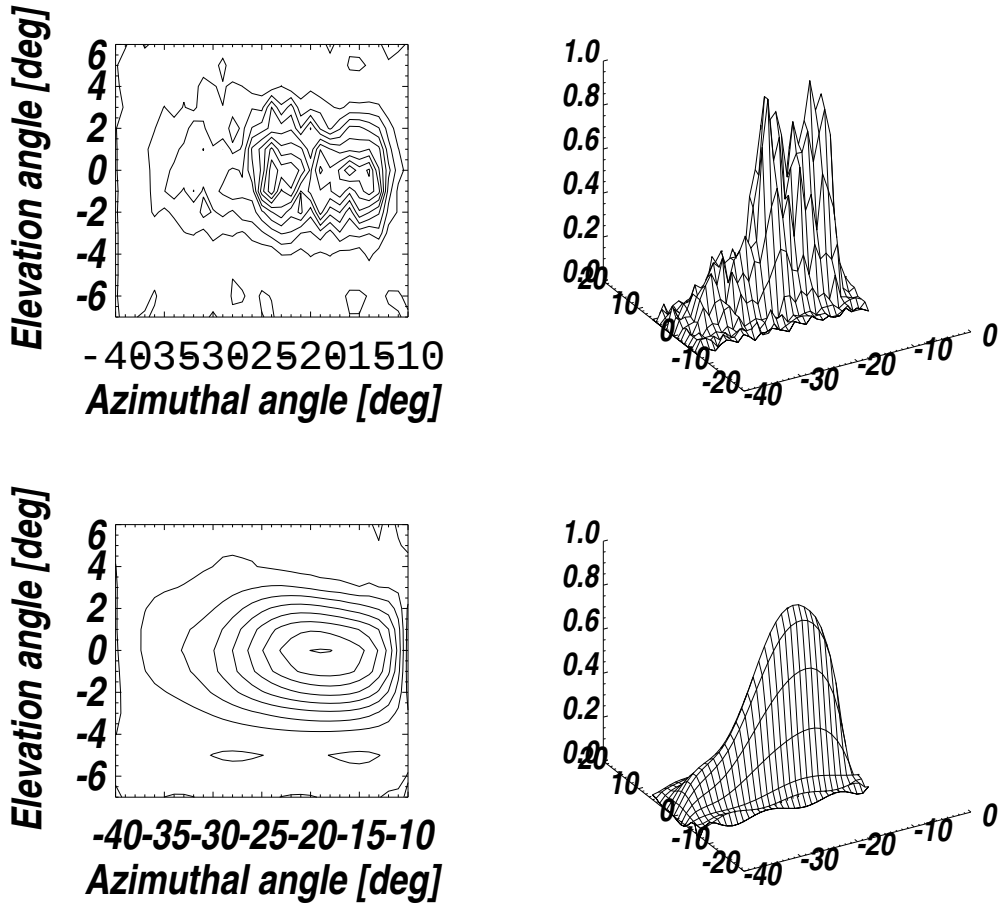

Figure 9: Angular scan of channel 14 at MCP bias 2400 V (top left and right) with corresponding fits (bottom left and right).

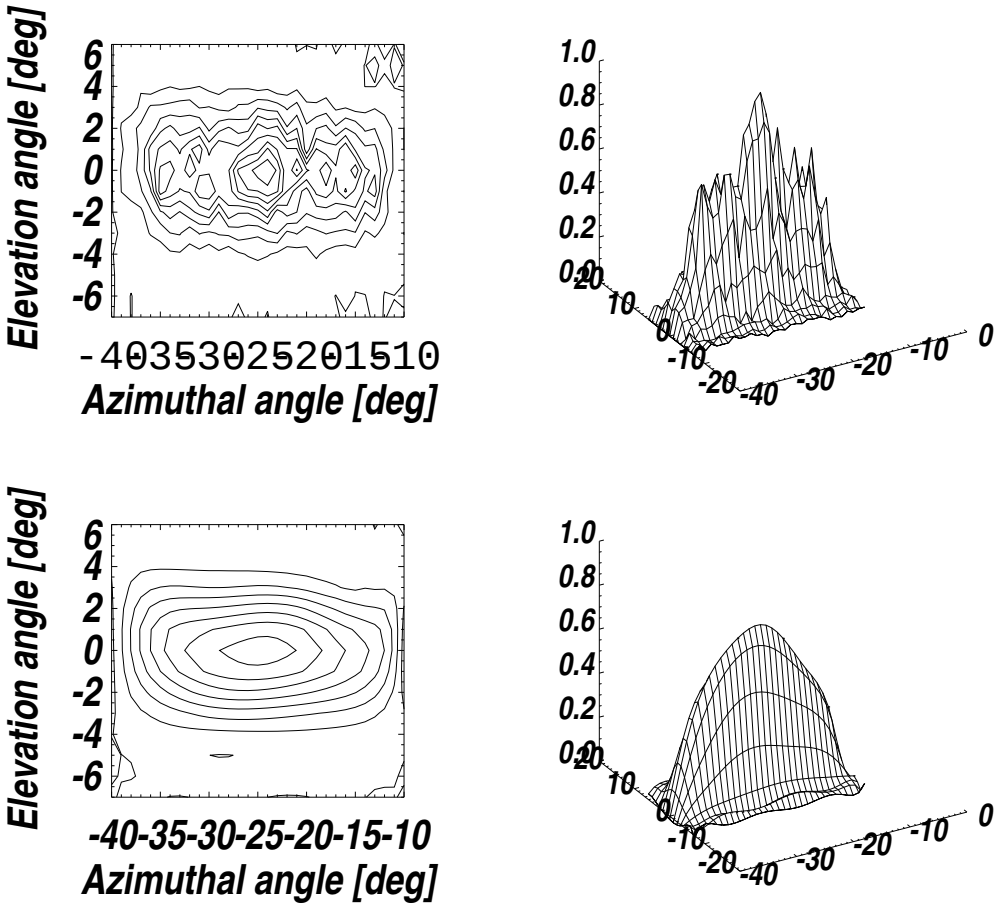

Figure 10: Angular scan of channel 14 at MCP bias 2500 V (top left and right) with corresponding fits (bottom left and right).

Table 4: Coefficients from angular response fit at MCP bias 2300 V.

$k_{i,j}$	$i=0$	$i=1$	$i=2$	$i=3$	$i=4$	$i=5$	$i=6$
$j=0$	-2.015E-03	2.378E-02	-2.206E-02	6.557E-03	-8.884E-04	5.728E-05	-1.427E-06
$j=1$	6.738E-03	1.029E-02	-2.483E-02	1.638E-02	-3.140E-03	2.363E-04	-6.210E-06
$j=2$	-1.634E-03	-7.846E-03	1.252E-02	6.948E-03	1.243E-03	-8.889E-05	2.225E-06
$j=3$	1.709E-04	1.673E-03	-2.302E-03	1.151E-03	-1.954E-04	1.336E-05	-3.190E-07
$j=4$	-7.717E-06	-1.310E-04	1.654E-04	-7.667E-05	1.232E-05	-7.951E-07	1.760E-08
$j=5$	1.438E-07	4.521E-06	-5.314E-06	2.281E-06	-3.431E-07	2.035E-08	-3.957E-10
$j=6$	-7.900E-10	-5.904E-08	6.557E-08	-2.606E-08	3.634E-09	-1.929E-10	2.996E-12

calculation. The center of channel 14 has the elevation and azimuth coordinates $\theta = 0°$ and $\varphi = -16.875°$. From the calibration measurements $C(0, -16.875) \approx 68$ and the effective target area of one channel in the NPI is $A_{eff} = 0.128\ cm^2$. Calibration measurements of instrument elevation and azimuth response gives:

$$\int_{\varphi} \int_{\theta} C(\theta, \varphi) \cos\theta d\theta d\varphi = 1.46$$

and from equation 4 this results in a geometrical factor of:

$$G_{sector} \approx \frac{0.128}{68} \cdot 1.46 = 2.7 \cdot 10^{-3} cm^2 sr$$

4 Instrument Configurations

Figures 11 and 12 shows the different instrument measurement configurations used in this report.

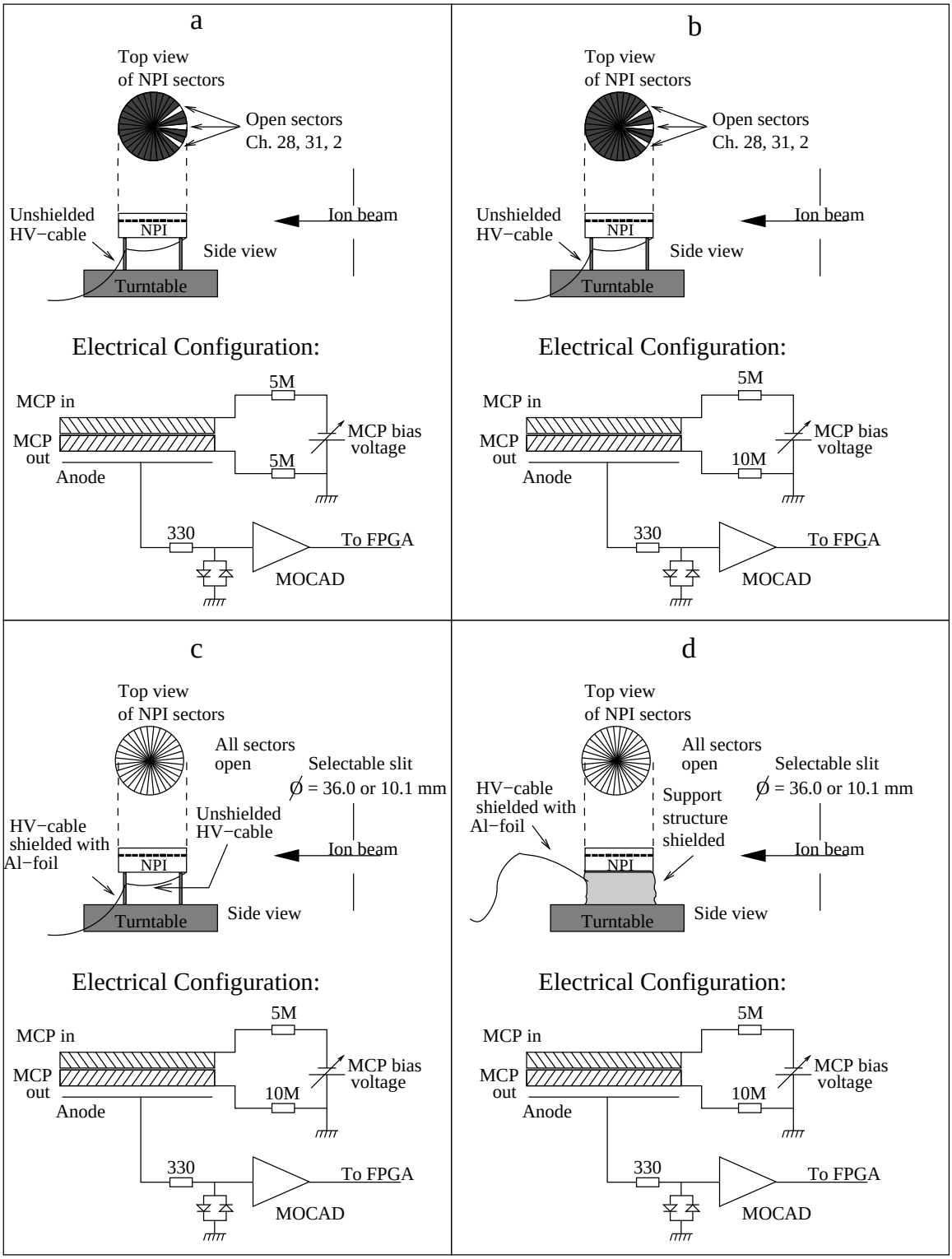

Figure 11: Instrument configurations.

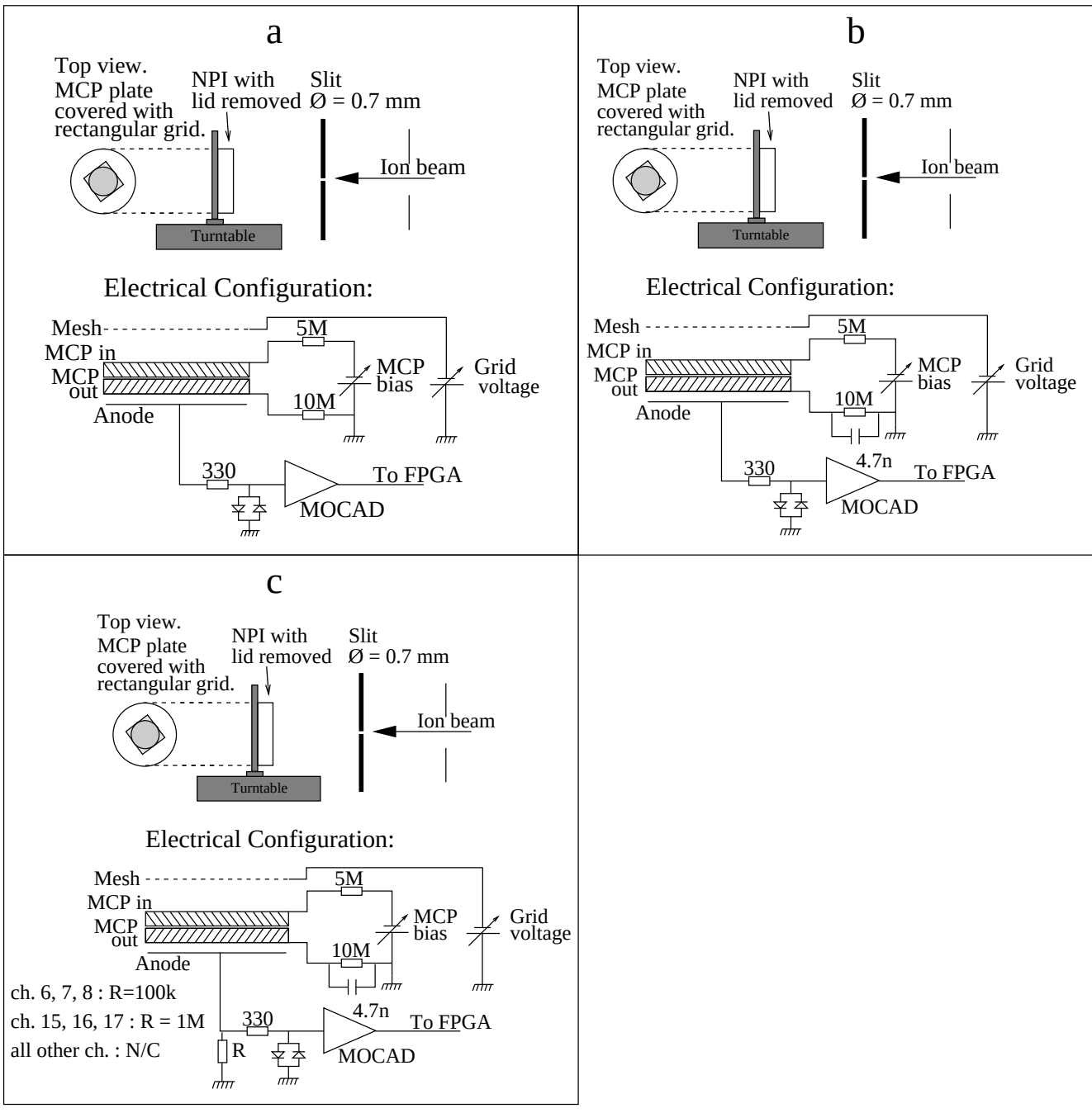

Figure 12: Instrument configurations.